Available online at www.sciencedirect.com
ScienceDirect
Journal of Energy Chemistry 24(2015)322–330
JOURNAL OF ENERGY CHEMISTRY
http://www.journals.elsevier.com/journal-of-energy-chemistry/

CO_2 adsorption performance of different amine-based siliceous MCM-41 materials

Zhilin Liu, Yang Teng, Kai Zhang*, Honggang Chen, Yongping Yang

Beijing Key Laboratory of Emission Surveillance and Control for Thermal Power Generation, North China Electric Power University, Beijing 102206, China

[Manuscript received November 24, 2014; revised January 14, 2015]

Abstract

A series of amine-based adsorbents were synthesized using siliceous MCM-41 individually impregnated with four different amines (ethylenediamine (EDA), diethylenetriamine (DETA), tetraethylenepentamine (TEPA) and pentaethylenehexamine (PEHA)) to study the effect of amine chain length and loading weight on their CO_2 adsorption performances in detail. The adsorbents were characterized by FT-IR, elemental analysis, and thermo-gravimetric analysis to confirm their structure properties. Thermo-gravimetric analysis was also used to evaluate the CO_2 adsorption performance of adsorbents. Longer chain amine-based materials can achieve higher amine loadings and show better thermal stability. The CO_2 adsorption capacities at different temperatures indicate that the CO_2 adsorption is thermodynamically controlled over EDA-MCM41 and DETA-MCM41, while the adsorption over TEPA-MCM41 and PEHA-MCM41 is under kinetic control at low temperature. The chain length of amines affects the CO_2 adsorption performance and the adsorption mechanism significantly. The results also indicate that CO_2 adsorption capacity can be enhanced despite of high operation temperatures, if appropriate amines (TEPA and PEHA) are applied. However, adsorbents with short chain amine exhibit higher adsorption and desorption rates due to the collaborative effect of rapid reaction mechanisms of primary amines and less diffusion resistance of shorter chain length amines.

Key words

amine-based MCM-41; CO_2 adsorption; chain length; adsorption mechanism; diffusion mechanism

1. Introduction

In the next few decades, fossil fuels will remain a major source of energy for years to come. CO_2 emissions from fossil fuel combustion have attracted more concern due to its important impact on global-warming [1]. For this reason the development of an effective means to capture CO_2 from flue gases is essential to cope with the worldwide demand of CO_2 reduction. Various methods have been proposed to capture CO_2, including cryogenic processes [2], absorption by aqueous solvents [3,4], membrane separation [5], and alkylamine solvents [6]. Ordered mesoporous silica, such as MCM-series [7,8], SBA-series [9,10] and HMS [11], possesses high surface areas, large and uniform pores, and tunable pore sizes as well as a large number of surface sites. These materials have been proven to be promising materials as catalysts and adsorbents. However, when they are used as adsorbents, physical adsorption tends to be insignificant under high temperature, which is the major drawback for CO_2 adsorption from flue gases. Because the amine groups can potentially enhance the CO_2-adsorbents interaction with high CO_2/N_2 selectivity [12] and can be operated at relatively high temperatures, a number of amine types have been investigated for impregnating or grafting them onto mesoporous silica materials to capture CO_2, due to the great potentials to create highly efficient materials as CO_2 adsorbents.

Many researchers approved that the CO_2 adsorption capacity was one of most critical factors to consider when measuring the performance of amine-based adsorbents [13,14]. The majority of published papers focused on the effect of amine groups on the CO_2 adsorption within the amine-loaded silica adsorbents. Recently, Hiyoshi et al. [15] and Knowles et al. [16] respectively used SBA-15 and HMS as substrates to synthesize amine-based adsorbents, including aminopropylsilyl-(AP-), ethylenediamine[propyl(silyl)]-(ED-) and diethylenetriamine[propyl(silyl)]-(DT-). Their results identified that the CO_2 adsorption capacity was a function of the amine content in the amine-based adsorbents, and

* Corresponding author. Tel: +86-10-61772413; Fax: +86-10-61772984; E-mail: kzhang@ncepu.edu.cn

This work was supported by the National Natural Science Foundation of China (91434120), the Fundamental Research Funds for the Central Universities (2014ZD06), and the 111 Project (No. B12034).

doi: 10.1016/S2095-4956(15)60318-7

the DT-functionalized material had a higher CO_2 adsorption capacity but lower amine efficiency than AP- or ED-functionalized materials. Hiyoshi et al. [9] also studied SBA-15 grafted with aminopropyltriethoxysilane (APS), N-(2-aminoethyl)-3-aminopropyl trimethoxysilane (AEAPS), and (3-trimetho-xysilylpropyl)diethylenetriamine (TA) separately, and found that the capacities of different amino silanes at the same surface density of amine were in the increasing order of APS>AEAPS>TA. Ko et al. [17] used (3-aminopropyl)trimethoxysilane (APTMS), [3-(methylamino)propyl]trimethoxysilane (MAPTMS), and [3-(diethyl-amino) propyl]trimethoxysilane (DEAPTMS) as amine source to explore the effect of primary, secondary, and tertiary amino silica adsorbents on CO_2 adsorption. The results confirmed that the adsorbed CO_2 was easily desorbed from the adsorbent in the order of tertiary>secondary>primary amino-adsorbents, while the adsorption capacity and the bonding-affinity increased in the reverse order. Furthermore, Serna-Guerrero et al. [18] also found that the increase of the CO_2 adsorption capacity correlated with the amine content. Using grafting method, a significant part of the pore volume remains unfilled despite of high amine loadings. In contrast, using impregnation, the extent of the amine functionalization depends on the total pore volume. Thus, in the latter case the amine may completely fill the pores [19]. However, the weight percentage of amines does not coincide with a corresponding benefit in other important parameters, such as thermal stability and/or adsorption rate, which may result from clogging or collapsing. Consequently, appropriate amine loading and amine chain length should be exercised and chosen when impregnating these amine groups into the substrates so as to make sure that the amine groups disperse evenly [20]. As mentioned above, many authors have suggested the potential importance of amine types and amine loading towards CO_2 adsorption capacity. Nevertheless, few studies investigated the adsorption mechanisms of different amine types related to amine chain length. Additionally, the CO_2 adsorption capacity is still far from the desired targets.

In this work, siliceous MCM-41 is chosen as the substrate. Although the scale-up of MCM-41 production is not available now in terms of its present cost, it is still a material of great potential due to its high surface area and regular periodic framework structure, as well as rapid gas diffusion rate. Moreover, the synthesis technology of MCM-41 is quite mature as well [7]. Four amines with gradual increasing chain length are used as the amine base to synthesis MCM-41 loaded amine with different amine loading. CO_2 adsorption capacity, adsorption rate and thermal stability of these amine-based adsorbents are studied. The work aims to discuss the effect of amine chain length on the CO_2 adsorption performance of amine-based MCM-41 and to explore the guiding principle for synthesizing appropriate adsorbents with higher CO_2 adsorption capacity which can be operated at higher temperature. The present study also contributes a fundamental understanding of the adsorption mechanisms and how the structure of amine groups affects the adsorption performance, which will further improve the CO_2 adsorption capabilities.

2. Experimental

2.1. Synthesis of amine-based MCM-41 adsorbents

Ethylenediamine (EDA), diethylenetriamin (DETA), tetraethylenepentamine(TEPA) and pentaethylenehexamine (PEHA) were used as the organic amine base in this study due to their gradual increasing amine chain lengths as listed in Table 1. Siliceous MCM-41 was prepared in the presence of cetyltrimethylammonium bromide (CTAB) and tetraethylorthosilicate (TEOS) according to the procedure reported in Ref. [21]. All of the amine-loaded materials were prepared by impregnation method. Typically, a desired amount of amine (EDA, DETA, TEPA, and PEHA) was dissolved in 10 mL dry ethanol. The mixture was stirred to make the amine be well dissolved, and then 0.5 g MCM-41 was added. The obtained slurry was continuously stirred at room temperature until sufficiently blended and then sealed to stand for 12 h in air, followed by drying for 8 h at 80 °C in a drying oven considering the boiling point of EDA of 116 °C. Hereafter, the amine-based samples with different amine loading were denoted as 10 wt%, 20 wt%, 40 wt%, 45 wt%, and 50 wt% EDA-MCM41, DETA-MCM41, TEPA-MCM41, and PEHA-MCM41, respectively.

Table 1. Four amines with different chain lengths used as amine sources in this work

Amine	Molecular weight (g/mol)	Density (g/mL)	Formula
Ethylenediamine (EDA)	60.10	0.90	$H_2NCH_2CH_2NH_2$
Diethylenetriamine (DETA)	103.17	0.96	$H_2NCH_2CH_2NHCH_2CH_2NH_2$
Tetraethylenepentamine (TEPA)	189.31	0.95	$NH_2(CH_2CH_2NH)_3CH_2CH_2NH_2$
Pentaethylenehexamine (PEHA)	232.30	1.00	$H_2N(C_2H_4NH)_5H$

2.2. Characterization

Elemental analysis was carried out using vario MACRO cube elemental analyzer (Elementar, German) to determine C, H and N contents in the samples. Infrared spectra of MCM-41 and amine-based MCM-41 were recorded in the $4000-450\,cm^{-1}$ region using Spectrum100FT-IR (PerkinElmer, USA).

Pore diameters and surface areas of the samples were evaluated via N_2 physical adsorption analysis using ASAP2020 (Micromeritics, USA). Each sample was degassed at 350 °C, 1.33 Pa under nitrogen flow for 5 h prior to

measurement. The N_2 adsorption data were recorded at the liquid nitrogen temperature (–196 °C). The surface areas and the pore size distributions were calculated by the BET and BJH equations. The total pore volume was calculated from the amount of adsorbed N_2 at the partial pressure $p/p_0 = 0.99$.

Thermo-gravimetric analysis (TA Instruments, USA) was applied to determine the loading amount of amine and the thermal stability of adsorbents. From a series of experiments, it is determined to treat the materials at 100 °C for a period of 60 min in N_2 to remove all the water and CO_2 adsorbed from the air. After the initial heat treatment, a heating rate of 10 °C·min^{-1} up to 700 °C in N_2 is conducted to calculate the real amine amount impregnated on substrates.

2.3. CO_2 adsorption

CO_2 adsorption and desorption measurements were also performed on thermogravimetric analysis at atmosphere pressure. A simulated gas mixture of 10% CO_2 and 90% N_2 was used as the model flue gas. In each run, about 3 mg adsorbent sample was loaded into an alumina sample pan, and then pretreated at 100 °C for 1 h in N_2 to remove the adsorbed moisture, followed by cooling to the adsorption temperature of 35 °C prior to its exposure to CO_2. The desorption run was conducted in a pure N_2 flow at 100 °C to achieve complete desorption [22−24]. Meanwhile, adsorption measurements at different temperatures (30, 35, 50, 70, 90 and 100 °C) at a heating rate of 1 °C/min were conducted to examine the effects of forward temperature sequencing on CO_2 adsorption capacities of amine-based materials, and then the temperatures decreased again to study the effects of backward temperature.

3. Results and discussion

3.1. Materials characterization

3.1.1. Materials structure

The average pore diameter and surface area of MCM-41 are 4.64 nm and 865 m^2·g^{-1} estimated using Barrett-Joiner-Halenda (BJH) method and Brunauer-Emmett-Teller (BET) surface area analysis, respectively.

The presence of surface functional groups of amine-based MCM-41 samples was confirmed by the FT-IR spectra. As shown in Figure 1(1), the band at 1634 cm^{-1} of the spectrum of MCM-41 can be attributed to the physical adsorbed water [25,26], and the bands between 400 and 1500 cm^{-1} arise from the frame vibration of MCM-41, including δ(Si–O–Si), ν_s(Si–O–Si) and ν_{as}(Si–O–Si) vibration stretch at 463, 807 and 1088 cm^{-1}, respectively [27]. Besides, the band at 3462 cm^{-1} is the characteristic of (Si–)OH stretch. The spectrum of EDA-MCM41 (Figure 1(2)) has two more bands of $\nu_s(CH_2)$ at 2852 cm^{-1} and $\delta(NH_2)$ at 1569 cm^{-1} compared with MCM-41, indicating the loading of EDA onto MCM-41 [28]. The bands at 1330, 1574 and 1625 cm^{-1} (Figure 1(3)) are characteristics of δ(C–N), δ(N–H) of –NH– and δ(N–H) of –NH_2 separately, which illustrates the presence of DETA, while the bands appearing at 1325, 1572 and 1624 cm^{-1} are corresponding to δ(C–N), δ(N–H) of –NH– and δ(N–H) of –NH_2 for the spectrum of TEPA-MCM41 (Figure 1(4)) [29–31]. Figure 1(5) shows the peaks of δ(C–N), δ(N–H) of –NH– and δ(N–H) of –NH_2 at 1317, 1550 and 1623 cm^{-1} and it indicates that PEHA is impregnated onto MCM-41. Each EDA molecule consists of two primary amines while the percentage of primary amines in DETA, TEPA or PEHA is lower than that in EDA. Consequently, the intensity of $\delta(NH_2)$ for EDA should be the maximum due to the highest concentrations of the primary amine. However, as illustrated in the Figure 1, the intensity of EDA is smaller than the other three, which may be due to relatively lower loading of EDA onto MCM-41.

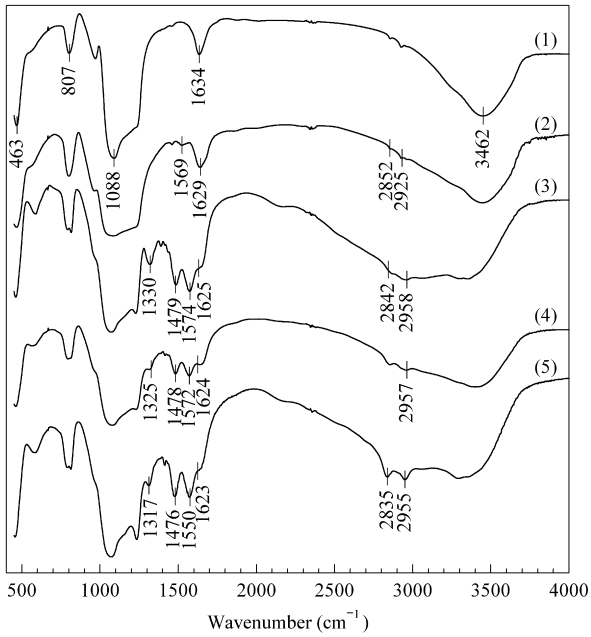

Figure 1. FTIR spectra of different amine-based adsorbents. (1) MCM-41, (2) EDA-MCM41, (3) TEPA-MCM41, (4) TEPA-MCM41, (5) PEHA-MCM41

The actual amine loadings of amine-based materials were determined by nitrogen content through elemental analysis. As shown in Figure 2, the trend of the amine loadings impregnated on MCM-41 is in accordance with the amine added, and the amine with long chain exhibits a slightly higher amine loading even with the same amount amines added. This difference may be ascribed to the impregnated species. Adsorbents prepared by impregnation have negligible covalent bonding occurring between amine constituents and substrates. The majority of the amine present within the interior pores of the substrates is held together by van der Waals forces. EDA and DETA which have lower molecular weight show lower melting points and they are less stable than PEHA during thermal desorption.

EDA-MCM41, DETA-MCM41, TEPA-MCM41 and PEHA-MCM41 with the amine loading of 40 wt% were

chosen to conduct the elemental analysis, and the results are listed in Table 2. Comparing the mass determined by TGA and elemental analysis, the relative error is less than 3.8%. EDA is partially lost during the impregnation process which is consistent with our previous work reported in Ref. [32].

Table 2. Elemental analysis of MCM-41 and amine-based MCM-41

Samples	C (%)	H (%)	S (%)	N (%)	C/N atomic ratio*	N content (mmol/g)
MCM-41	2.01	0.56	0.07	0.26		0.18
EDA-MCM41	8.58	2.55	0.10	6.04	1.27 (1.0)	4.32
DETA-MCM41	15.25	3.85	0.08	9.09	1.67 (1.3)	6.50
TEPA-MCM41	19.32	4.81	0.10	10.22	1.98 (1.6)	7.30
PEHA-MCM41	19.38	5.07	0.12	11.19	1.81 (1.7)	8.00

* Data presented in parentheses are the corresponding theoretical C/N atomic ratios

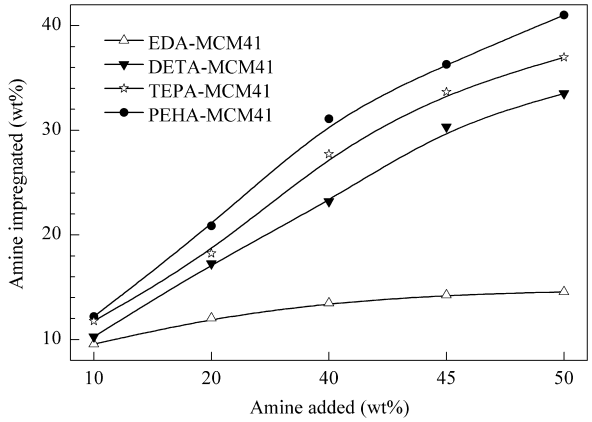

Figure 2. Calculated amine content versus actual amine content for amine-impregnated materials

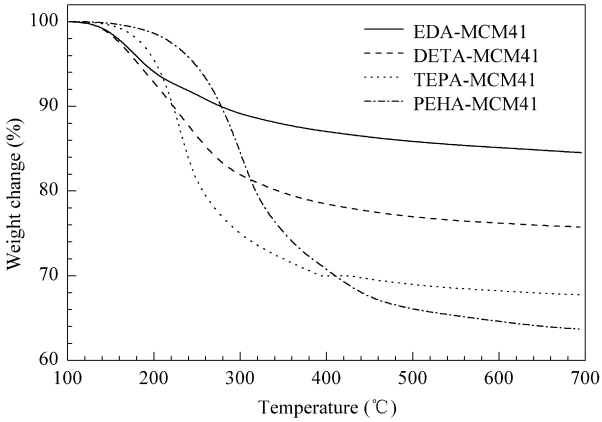

Figure 3. TG curves of samples

3.1.2. Thermal stability

Thermo-gravimetric analysis (TGA) was used to determine the operating temperature under which no decomposition of the impregnated amine could happen. Taking 40 wt% amine-based MCM-41 as an example, Figures 3 and 4 show the TG (thermo-gravimetric) and DTG (differential thermo-gravimetric analysis) curves of the four adsorbents.

All the samples were kept at 100 °C for 1 h to remove the surface moisture first. Figure 3 shows that the amine-based adsorbents exhibit different weight losses at the final temperature with an order of EDA-MCM41<DETA-MCM41<TEPA-MCM41<PEHA-MCM41, and the numbers are 13.48%, 23.20%, 27.72% and 31.09%, respectively. The weight loss reflects the amine loading amount after impregnation. However, the weight losses of all materials are less than the amount of amine added, indicating that amine partially volatilize in the synthesis process. Only 13.48% weight loss of EDA-MCM41 is obtained which further suggests that EDA is volatilized during preparation. Considering the boiling points of EDA(116 °C), DETA(207 °C), TEPA(340 °C) and PEHA(380 °C), amines with higher boiling point are more stable, which is beneficial for future industrial utilization.

Figure 4 shows that the decomposition of EDA starts at 102 °C and reaches the maximum weight loss rate of ∼0.10 wt%·min^{-1} at 177 °C. At temperature above 220 °C, the rate of weight loss increases again, which may be ascribed as a different decomposition process in which the decomposition of the amines coated outside the pores and filled inside the pores [33]. With further increasing temperature, the rate of weight loss decreased again, implying that all the amine molecules impregnated on MCM-41 decomposed completely. For DETA-MCM41, TEPA-MCM41 and PEHA-MCM41, the initial decomposition temperatures are 116 °C, 135 °C and 151 °C, and the corresponding rates of weight loss reach the maximum at 202 °C, 231 °C and 300 °C, respectively. The longer the amine chain length is, the higher the initial decomposition temperature and the maximum weight loss temperature Therefore, the thermal stability closely correlates with the increase of the amine chain length. It should be noted that the longer chain amine molecules are not located inside the pores, but aggregate like solid amine. The existence of amine covering the external surface of MCM-41 increases the resistance to the decomposed product diffusion and heat transfer [33]. In addition, the rate of weight loss of TEPA-MCM41 is greater, and the temperature range is significantly narrower, relative to the other three materials. This difference can be attributed to the uniform dispersion of TEPA into the mesoporous channel and that the bonds between TEPA and MCM-41 are easily

destroyed at temperature between 200−300 °C. Overall, the impregnated amine species seems to be thermally stable up to below 100 °C, and the thermal stability increases with the amine chain length.

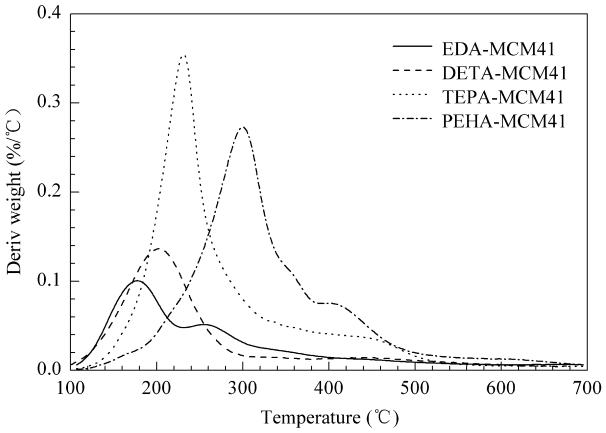

Figure 4. DTG curves of samples

3.2. CO_2 capacity

3.2.1. Effect of amine chain length on amine loading

Our preliminary TG experiments illustrate that the materials have no particular affinity to N_2 over the temperature range from 35 to 100 °C, so the adsorption capacity of N_2 is negligible. On the other hand, the CO_2 adsorption capacity of original MCM-41 is 0.61 mmol/g, indicating that the substrate is capable of adsorbing CO_2.

The adsorption and desorption curves of 40% amine loading materials are shown in Figure 5. It can be seen that the slopes of adsorption and desorption curves for the synthesized materials are different. EDA-MCM41 and DETA-MCM41 exhibit faster adsorption kinetics, while TEPA-MCM41 and PEHA-MCM41 need more time to reach equilibrium. However, TEPA-MCM41 and PEHA-MCM41 possess higher adsorption capacity. Upon rapid heating to 100 °C in pure N_2, EDA-MCM41 and DETA-MCM41 quickly desorb all the CO_2 which is adsorbed in previous process. The adsorption rates of EDA-MCM41 and DETA-MCM41 are faster than TEPA-MCM41 and PEHA-MCM41, which will be further discussed in section 3.2.3.

The adsorption and desorption experiments were conducted three times to calculate the average adsorption capacity. Through calculation, the saturation capacities as a function of theoretical amine loading are summarized in Figure 6. The maximum CO_2 adsorption capacities of EDA-MCM41, DETA-MCM41, TEPA-MCM41 and PEHA-MCM41 are 1.19 mmol/g, 1.43 mmol/g, 1.96 mmol/g and 2.34 mmol/g, respectively, and the standard deviations are not more than 6.3%. The highest capacities all appear at amine loading of 40 wt%, however, the adsorption capacities of 20 wt%, 30 wt% and 50 wt% EDA-MCM41 show the same level as 40 wt% EDA-MCM-41. For the amine-based MCM-41, the amine sites are the main active sites to adsorb CO_2 molecules [34]. However, when the amine loading increases to a certain amount, the inner pore surface is entirely filled and the excess amine coats the outer surface, which limits the interaction between CO_2 and amine inside the pores due to the mass transfer resistance. Also, the increasing organic steric hindrance may also result in a decrease of the adsorption capacity [9,35]. All of these reasons contribute to the decrease of the adsorption capacity for 50 wt% amine-based MCM-41 adsorbents.

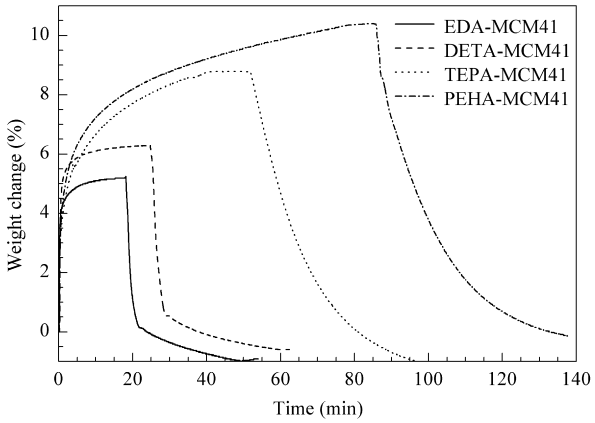

Figure 5. CO_2 adsorption and desorption curves obtained with 10% CO_2/90% N_2 for different samples

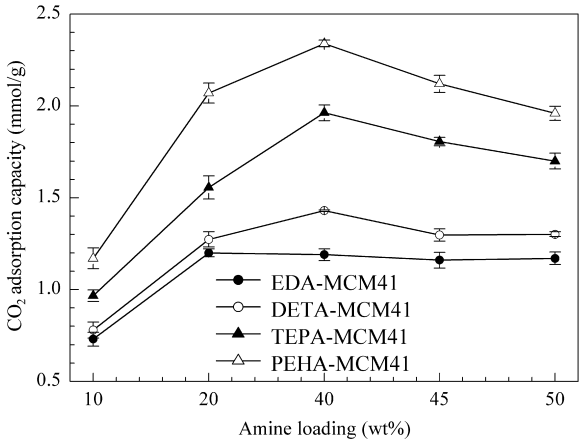

Figure 6. CO_2 adsorption capacity as a function of nominal amine loading for different samples

The interaction between CO_2 and amines is thought to have three mechanisms as illustrated in Schemes (1−3). Caplow [35] described the zwitterionic mechanism of a primary amine with CO_2 for the formation of carbamate. Firstly, the lone pair NH_2 on the amine attacks CO_2 to form the CO_2-amine zwitterions. A free base deprotonates the zwitterion and forms the carbamic acid and ammonium carbamate salt. With the above consideration, each molecule of CO_2 could bond to two nearby primary amine sites on EDA-MCM41 to form an ammonium carbamate species in an anhydrous CO_2 flow as depicted in Scheme 1. Secondly, Scheme 2

shows that the CO_2 adsorption process may act via the intramolecular acid-base balance with the secondary amine on the same sites. Thirdly, Scheme 3 demonstrates the possible procedure of CO_2 capture by two secondary amines [17]. One CO_2 molecule reacts with a secondary amine site to form ammonium carbamate directly. For DETA-MCM41, TEPA-MCM41 and PEHA-MCM41, the above-mentioned three mechanisms may occur simultaneously.

Table 3. Comparison of 40 wt% amine-based MCM-41 in capacity and amine efficiency

Adsorbent	Amine molecule (nm^2)	CO_2 adsorption capacity ($mmol \cdot g^{-1}$)	CO_2/N ratio	CO_2 adsorbed by each amine molecule (mmol)
EDA-MCM41	1.31	1.19	0.28	0.09
DETA-MCM41	1.45	1.43	0.22	0.11
TEPA-MCM41	0.98	1.96	0.27	0.22
PEHA-MCM41	0.87	2.34	0.29	0.28

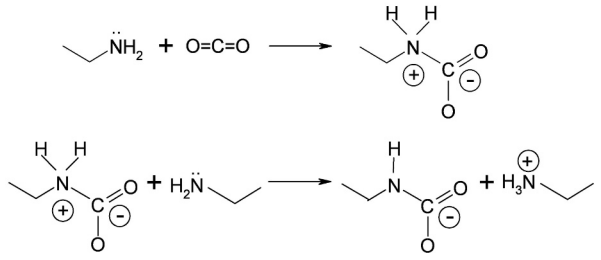

Scheme 1. Mechanism for the reaction of CO_2 with two NH_2

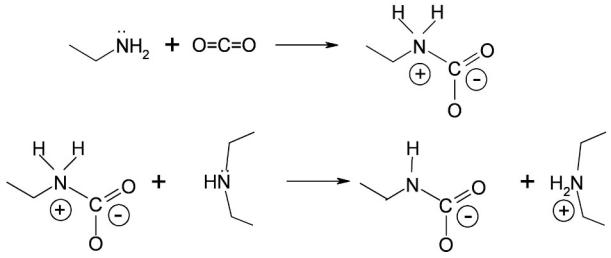

Scheme 2. Mechanism for the reaction of CO_2 with NH_2 and NH

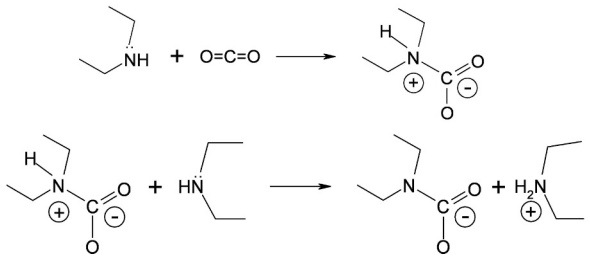

Scheme 3. Mechanism for the reaction of CO_2 and two NH

The amounts of CO_2 adsorbed by each molecule for EDA-MCM41, DETA-MCM41, TEPA-MCM41 and PEHA-MCM41 are 0.09, 0.11, 0.22 and 0.28 mmol respectively, as listed in Table 3. It is worth noting that the amounts are well consistent with the amine sites occupied by each amine molecule. The value of CO_2/N ratio listed in Table 3 reflects the adsorption efficiency in terms of active sites capable of reacting with CO_2. With the assumption of carbamate formation, the maximum CO_2/N molar ratio should be 0.5 under dry conditions, and considering the physical adsorption capacity of MCM-41 carriers, this ratio should be higher than 0.5. However, the current results show that the maximum CO_2/N ratios are no more than 0.3 for all samples.

For amine impregnated materials, the CO_2/N ratios reported in literatures vary over a wide range. Franchi et al. [36] obtained a CO_2/N ratio of 0.40 with a diethanolamine modified PE-MCM-41 sample. Wei et al. [14] obtained CO_2/N ratios of 0.25, 0.21 and 0.27 using MCM-41 substrate with DETA, TEPA and 2-amino-2-methyl-1-propanol, respectively. Lin et al. [37] impregnated TEPA on MPS and reported that the CO_2/N ratio reached 0.72. In this work, the CO_2/N ratio ranges from 0.27 to 0.36 for EDA-MCM41, 0.14 to 0.28 for DETA-MCM41, 0.18 to 0.34 for TEPA-MCM41 and 0.20 to 0.45 for PEHA-MCM41 as a function of amine loading.

The actual CO_2/N ratios obtained are significantly below 0.5 which may be ascribed to following reasons. First, some amine molecules are isolated from each others due to steric effects, and the long organic chains cover a part of the N atom of the amine and hinder the access of CO_2 molecules. Secondly, CO_2 adsorbed by amine is weakly sensitive to the low partial pressure of CO_2 (1.0 kPa) used in this work. Furthermore, the lone electron pairs present on the N atoms interact with hydrogen atoms to form hydrogen bonds, which results in decreased activity [23]. The presence of the amine forming hydrogen bonds could prevent the amine reacting with CO_2. Lastly, effective CO_2 adsorption sites seem to be the densely anchored amine species, perhaps not the isolated amines as suggested in Ref. [17].

Additionally, Knowles et al. [16] supposed that the primary amine is more effective than the secondary amine. As listed in Table 3, the CO_2/N ratio of EDA-MCM41 (100% primary amine) is 0.28, larger than that of DETA-MCM41 (67% primary amine), TEPA-MCM41 (40% primary amine) for the identical amine added. However, the CO_2/N ratio of PEHA-MCM41 is 0.29 while the content of primary amine is 33%, so the influence may be caused by several competitive factors.

3.2.2. Effect of temperature on diffusion mechanism

To investigate the effect of temperature on the diffusion mechanism and CO_2 adsorption capacities of amine-based materials, the adsorption experiments are conducted by TGA with the temperature stepwise rising from 30 °C to 100 °C, and then stepwise cooling down to 30 °C under 10% CO_2 and

90% N_2 flow of 60 mL/min.

Song et al. [38,39] speculated that CO_2 adsorption on amine-based molecular sieves may include both physical adsorption within pores and chemical adsorption on amine groups. As shown in Figure 7, with the increase of temperature from 30 to 100 °C, the CO_2 adsorption capacities of EDA-MCM41 and DETA-MCM41 decline while those of TEPA-MCM41 and PEHA-MCM41 have an opposite tendency. At lower temperatures the CO_2 molecules diffuse and interact with the bulk amine for both EDA-MCM41 and DETA-MCM41 adsorbents. When the temperature increases, the adsorbed CO_2 molecules within the bulk amine are easy to escape from the sites due to the lower diffusion barrier. CO_2 adsorbed on the amine surface becomes unfavorable at higher temperatures because the kinetic effects have less influence than thermodynamic effects. When the temperature is subsequently decreased from 100 to 30 °C under the same CO_2 flow, the adsorption capacities of EDA-MCM41 and DETA-MCM41 increase which further supports that the adsorption on EDA-MCM41 is controlled by thermodynamics.

For TEPA-MCM41 and PEHA-MCM41, the adsorption capacity correlates with temperatures and their maximum CO_2 adsorption capacities can be achieved within a temperature range of 70 to 90 °C. Here, the positive effects of higher temperature on the adsorption (such as the increase of mobility in the pores, reaction kinetics and CO_2 diffusion) overweight the negative effects (such as the exothermic nature of physical and chemical adsorption over amine groups) [20]. When the temperature increased to 100 °C the adsorption capacities declined, indicating that the adsorption becomes thermodynamically unfavorable. However, when the temperature subsequently decreased from 100 to 30 °C under the same CO_2 flow, the adsorption capacities would increase with the backward temperature. At high temperature, CO_2 molecules diffuse and interact with the amine bulk. When the temperature decreases, the adsorbed CO_2 molecules within the amine bulk are not able to escape from the sites due to the high diffusion barrier and thus store inside. On the other hand, CO_2 adsorbed on the amine surface becomes more favorable with the decrease of temperature. Thus, higher adsorption capacities can be obtained at lower temperature. This result confirms that CO_2 adsorption over amine-based materials is under kinetic control when the temperature is below 90 °C and amines with long chain have larger diffusion resistance. Higher energy is required to break the bond. The low adsorption capacities at low temperature are the result of the low adsorption rate. Moreover, high adsorption capacity could be attained if the adsorption time is extended long enough [33].

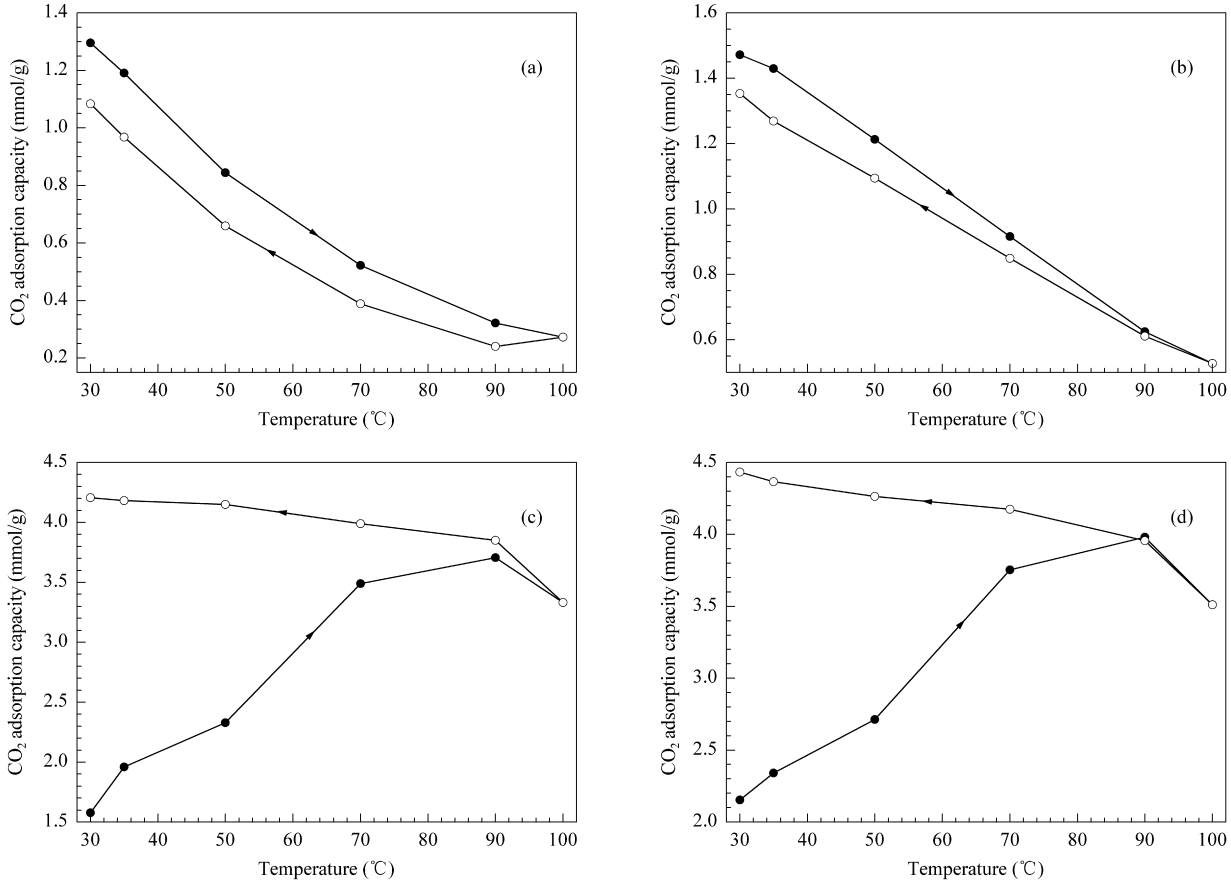

Figure 7. CO_2 adsorption capacity of 40 wt% (a) EDA-MCM41, (b) DETA-MCM41, (c) TEPA-MCM41 and (d) PEHA-MCM41 versus adsorption temperature with increasing (●) and decreasing (○) temperature

3.2.3. Adsorption rate and desorption rate

Due to the low adsorption rate, most experiments could only achieve partial bed saturation capacity. Therefore, the study of adsorption and desorption rate is equally (if not more) important. As shown in Figure 5, the adsorption and desorption rates are different. In order to further analyze the adsorption and desorption rate, the fractional CO_2 adsorption is defined and compared with four 40 wt% amine-based adsorbents previously described. The dynamic data is calculated based on the adsorption capacity versus time:

$$\text{Fractional } CO_2 \text{ adsorption} = \frac{\text{Adsorption capacity at time } t}{\text{Adsorption capacity at equilibrium}} \quad (1)$$

Figure 8 demonstrates that TEPA-MCM41 and PEHA-MCM41 show the slow increase of fractional CO_2 adsorption curve, whereas EDA-MCM41 and DETA-MCM41 exhibit the rapid adsorption rate response. In the initial 1 min exposure to CO_2, the fractional CO_2 adsorption order is EDA-MCM41>TEPA-MCM41>PEHA-MCM41>DETA-MCM41. After this point, DETA-MCM41 performs higher fractional adsorption than TEPA-MCM41 and PEHA-MCM41. In the initial 15 mins, EDA-MCM41 and DETA-MCM41 outperform TEPA-MCM41 and PEHA-MCM41. This is beneficial when applying the material to separate CO_2 in a rapid (cycle time of <1.0 min) or ultra rapid (cycle time of <5 s) cyclic adsorption process. Within 15 min, EDA-MCM41 and DETA-MCM41 could achieve 92% and 91% of the total equilibrium CO_2 capacity, but for TEPA-MCM41 and PEHA-MCM41, the percentages are only around 60%.

Figure 9 supplementarily shows that the increase of rate contributes to CO_2 adsorption in the initial exposure time. When the four materials are compared, the fractional uptake of EDA-MCM41 and DETA-MCM41 outperform the other two adsorbents. This behavior demonstrates that the dynamic performances of EDA-MCM41 and DETA-MCM41 are superior over TEPA-MCM41 and PEHA-MCM41. Moreover, the desorption performance of EDA-MCM41 and DETA-MCM41 (as description in Figure 5) are also rapid and could complete at 100 °C in pure N_2. Typically, less than 5 mins of purge at 100 °C is enough to entirely regenerate the adsorbents and it means low energy consumption for the regeneration of EDA-MCM41 and DETA-MCM41 adsorbents.

Ko et al. [17] reported that the slow increase of the adsorption slope presents the smooth bond between CO_2 and amines, and the rapid increase of the desorption curve is due to the weak bond between CO_2 and amines. However, in our results, for EDA-MCM41 and DETA-MCM41, the fractional CO_2 adsorption and fractional CO_2 desorption are all faster than TEPA-MCM41 and PEHA-MCM41 which is not consistent with their assumption. It can be concluded that in the adsorption process, for TEPA-MCM41 and PEHA-MCM41, the lag in the adsorption curve is not only the slow secondary mechanism of CO_2 adsorption but also the diffusion resistance of long chain length. Meanwhile, in the desorption procedure, the delays are the result of the mass transfer resistance caused by long amine chain length. Therefore, at the initial time, TEPA-MCM41 and PEHA-MCM41 encounter a greater resistance of mass transfer and then demonstrate a delay in the adsorption curve. From the discussion above, the good CO_2 adsorption and desorption performance of EDA-MCM41 and DETA-MCM41 is mainly due to the combined effects of rapid reaction mechanism of primary amine and decreased diffusion resistance of short chain length amines.

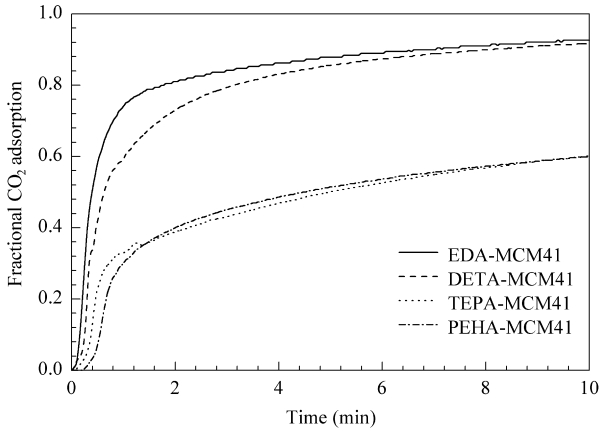

Figure 8. Comparison of the dynamic 10% CO_2/N_2 fractional uptake of different samples

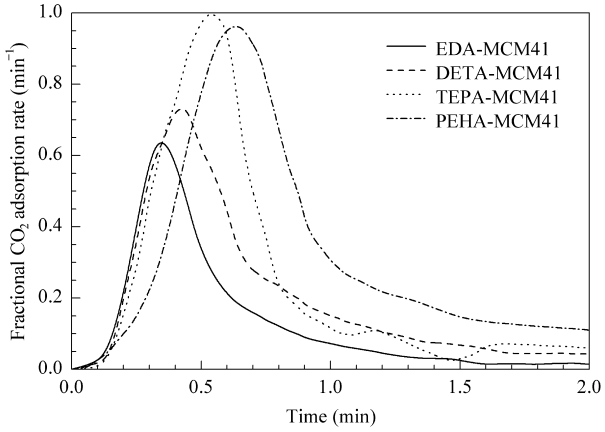

Figure 9. Comparison of the fractional adsorption rate of different samples

4. Conclusions

In this work, the adsorption of CO_2 over amine-based MCM-41 materials with gradual increasing amine chain length has been studied. FT-IR, elemental analysis and thermo-gravimetric analysis are used to characterize the materials structures and thermal stabilities. Thermo-gravimetric analysis is used to evaluate the CO_2 adsorption and desorption performance.

There is a significant positive correlation between the actual amine contents of synthesized adsorbents and the amounts of added amine; longer chain leads to slightly higher

amine loadings on the substrates and thus higher CO_2 adsorption capacities. The highest CO_2 adsorption capacity of 2.34 mmol/g is attained over 40 wt% PEHA-MCM41 while 20 wt% PEHA-MCM41 shows the highest CO_2/N ratio of 0.45, which is due to the better amine dispersion and lower diffusion barrier.

The adsorption performance at different temperatures reveals that CO_2 adsorption over TEPA-MCM41 and PEHA-MCM41 are under kinetic control while EDA-MCM41 and EDTA-MCM41 are under thermodynamic control below 90 °C. For amine-based adsorbents with longer amine chain, CO_2 adsorption capacities becomes much less susceptible to the temperature increase and even increase with the temperature until 90 °C.

In terms of dynamic CO_2 adsorption and desorption performance, amine-impregnated adsorbents with short amine chain exhibit higher adsorption and desorption rates and it is mainly attributed to the combined effect of rapid reaction mechanism of primary amine and the less diffusion resistance of short chain length.

Acknowledgements

Authors gratefully acknowledge the National Natural Science Foundation of China (91434120), Fundamental Research Funds for the Central Universities (2014ZD06), and the 111 Project (No. B12034).

References

[1] Monastersky R. *Nature*, 2009, 458(7242): 1091
[2] Zanganeh K E, Shafeen A, Salvador C. *Energy Procedia*, 2009, 1(1): 247
[3] von Harbou I, Hoch S, Mangalapally H P, Notz R, Sieder G, Garcia H, Spuhl O, Hasse H. *Chem Eng Process*, 2014, 75: 81
[4] Hasib-ur-Rahman M, Siaj M, Larachi F. *Chem Eng Process*, 2010, 49(4): 313
[5] Brunetti A, Scura F, Barbieri G, Drioli E. *J Membrane Sci*, 2010, 359(1-2): 115
[6] Araki S, Doi H, Sano Y, Tanaka S, Miyake Y. *J Colloid Interface Sci*, 2009, 339(2): 382
[7] Xu X C, Song C S, Andresen J M, Miller B G, Scaroni A W. *Microporous Mesoporous Mater*, 2003, 62(1-2): 29
[8] Kim S, Ida J, Guliants V V, Lin J Y S. *J Phys Chem B*, 2005, 109(13): 6287
[9] Hiyoshi N, Yogo K, Yashima T. *Microporous Mesoporous Mater*, 2005, 84(1-3): 357
[10] Gargiulo N, Peluso A, Aprea P, Pepe F, Caputo D. *J Chem Eng Data*, 2014, 59(3): 896
[11] Knowles G P, Graham J V, Delaney S W, Chaffee A L. *Fuel Process Technol*, 2005, 86(14-15): 1435
[12] Wang K, Shang H Y, Li L, Yan X L, Yan Z F, Liu C G, Zha Q F. *J Nat Gas Chem*, 2012, 21(3): 319
[13] Zhao W Y, Zhang Z, Li Z S, Cai N S. *Ind Eng Chem Res*, 2013, 52(5): 2084
[14] Wei J W, Liao L, Xiao Y, Zhang P, Shi Y. *J Environ Sci Chin (Huanjin Kexue Xuebao)*, 2010, 22(10): 1558
[15] Hiyoshi N, Yogo K, Yashima T. *Chem Lett*, 2004, 33(5): 510
[16] Knowles G P, Delaney S W, Chaffee A L. *Ind Eng Chem Res*, 2006, 45(8): 2626
[17] Ko Y G, Shin S S, Choi U S. *J Colloid Interface Sci*, 2011, 361(2): 594
[18] Serna-Guerrero R, Da'na E, Sayari A. *Ind Eng Chem Res*, 2008, 47(23): 9406
[19] Deshpande R S, Sharp-Goldman S L, Bocarsly A B. *Langmuir*, 2002, 18(20): 7694
[20] Sanz-Perez E S, Olivares-Marin M, Arencibia A, Sanz R, Calleja G, Maroto-Valer M M. *Int J Greenh Gas Con*, 2013, 17: 366
[21] Xu R R, Pang X Q. Chemistry: Zeolites and Porous Materials. Beijing: Science Press, 2004. 68
[22] Harlick P J E, Sayari A. *Ind Eng Chem Res*, 2006, 45(9): 3248
[23] Harlick P J E, Sayari A. *Ind Eng Chem Res*, 2007, 46(2): 446
[24] Kim S N, Son W J, Choi J S, Ahn W S. *Microporous Mesoporous Mater*, 2008, 115(3): 497
[25] Zhao H L, Hu J, Wang J J, Zhou L H, Liu H L. *Acta Physico-Chimica Sinica*, 2007, 23(6): 801
[26] Wang X R, Li H Q, Liu H T, Hou X J. *Microporous Mesoporous Mater*, 2011, 142(2-3): 564
[27] Liu L C, Li H Q, Zhang Y. *Catal Today*, 2006, 115(1-4): 235
[28] Kang P P, Song W S, Han B B, Xu S S. *Chin J Org Chem (Youji Huaxue)*, 2009, 29(6): 904
[29] Yue M B, Sun L B, Cao Y, Wang Y, Wang Z J, Zhu J H. *Chem Eur J*, 2008, 14(11): 3442
[30] Khatri R A, Chuang S S C, Soong Y, Gray M. *Ind Eng Chem Res*, 2005, 44(10): 3702
[31] Khatri R A, Chuang S S C, Soong Y, Gray M. *Energ Fuel*, 2006, 20(4): 1514
[32] Liu Z L, Teng Y, Zhang K, Cao Y, Pan W P. *J Fuel Chem Technol (Ranliao Huaxue Xuebao)*, 2013, 41(4): 469
[33] Wang X X, Ma X. L, Song C S, Locke D R, Siefert S, Winans R E, Möllmer J, Lange M, Mäller A, Gläser R. *Microporous Mesoporous Mater*, 2013, 169: 103
[34] Liu Q, Shi Y, Zheng S D, Ning L Q, Ye Q, Tao M N, He Y. *J Energ Chem*, 2014, 23(1): 111
[35] Caplow M. *J Am Chem Soc*, 1968, 90(24): 6795
[36] Franchi R S, Harlick P J E, Sayari A. *Ind Eng Chem Res*, 2005, 44(21): 8007
[37] Lin L Y, Bai H L. *Microporous Mesoporous Mater*, 2010, 136(1-3): 25
[38] Wang X X, Schwartz V, Clark J C, Ma X L, Overbury S H, Xu X C, Song C S. *J Phys Chem C*, 2009, 113(17): 7260
[39] Ma X L, Wang X X, Song C S. *J Am Chem Soc*, 2009, 131(16): 5777